AUTHOR QUERY FORM

AIP Publishing	**Journal: J. Chem. Phys.** **Article Number: JCP19-AR-01440**	**Please provide your responses and any corrections by annotating this PDF and uploading it to AIP's eProof website as detailed in the Welcome email.**

Dear Author,

Below are the queries associated with your article. Please answer all of these queries before sending the proof back to AIP.

Article checklist: In order to ensure greater accuracy, please check the following and make all necessary corrections before returning your proof.
1. Is the title of your article accurate and spelled correctly?
2. Please check affiliations including spelling, completeness, and correct linking to authors.
3. Did you remember to include acknowledgment of funding, if required, and is it accurate?

Location in article	Query/Remark: click on the Q link to navigate to the appropriate spot in the proof. There, insert your comments as a PDF annotation.
Q1	Please check that the author names are in the proper order and spelled correctly. Also, please ensure that each author's given and surnames have been correctly identified (given names are highlighted in red and surnames appear in blue).
Q2	Figures must be cited in numerical order; therefore, we have renumbered Figs. 7–9 and 6 as 6–9. Please check.
Q3	There were no equations numbered (9)–(11) in your paper; hence, we have renumbered Eqs. (13)–(15) as Eqs. (9)–(11). Please check all renumbering carefully throughout.
Q4	Reference 65 cited in Table IV does not have a corresponding reference on the reference list. Please provide reference details and insert the corresponding citation accordingly.
Q5	Reference 50 was not cited in text. We have inserted a citation in the sentence beginning "At short times...." Please check our placement and reposition if necessary.
Q6	In the caption of Fig. 9, please check whether "interferometric experimental of" could be changed as "interferometric experimental data of."
Q7	The order of source files for the subfigures of Fig. 10 did not match the order of figures that appeared in your manuscript. We have followed the source files for the order of figures. Please check and confirm.
Q8	Acronyms "SST + TC" and "SST + TG" have both been used for the definition "SST and thermogravitational column experiments" in different occurrences. Please check.
Q9	There were two tables numbered (V) in your paper; hence, we have changed the repeated number to (VI) and renumbered all subsequent equations accordingly. Please check all renumbering and update the citations in the text as needed.
Q10	Please confirm the change in volume number in Ref. 2.
Q11	References 3 and 18 contain identical information. Please check and provide the correct reference or delete the duplicate reference. If the duplicate is deleted, renumber the reference list as needed and update all citations in the text.
Q12	We were unable to locate a digital object identifier (doi) for Ref. 17. Please verify and correct author names and journal details (journal title, volume number, page number, and year) as needed and provide the doi. If a doi is not available, no other information is needed from you. For additional information on doi's, please select this link: http//www.doi.org/.
Q13	Please provide publisher's name in Ref. 28.

Continued on next page.

Continued from previous page.	
	Please confirm ORCIDs are accurate. If you wish to add an ORCID for any author that does not have one, you may do so now. For more information on ORCID, see https://orcid.org/. Quentin Galand – 0000-0001-5922-8585 Stéfan Van Vaerenbergh – 0000-0002-6614-0458 Werner Köhler – Oleg Khlybov – Tatyana Lyubimova – Aliaksandr Mialdun – 0000-0002-7787-2865 Ilya Ryzhkov – Valentina Shevtsova – 0000-0001-6109-5048 Thomas Triller – 0000-0002-7763-7865 Please check and confirm the Funder(s) and Grant Reference Number(s) provided with your submission: European Space Agency, Award/Contract Number AO-2009-0858/1056 Deutsches Zentrum für Luft- und Raumfahrt, Award/Contract Number 50WM1544, 50WM1130 Please add any additional funding sources not stated above.

Thank you for your assistance.

The Journal of Chemical Physics ARTICLE scitation.org/journal/jcp

Results of the DCMIX1 experiment on measurement of Soret coefficients in ternary mixtures of hydrocarbons under microgravity conditions on the ISS

Cite as: J. Chem. Phys. 151, 000000 (2019); doi: 10.1063/1.5100595
Submitted: 23 April 2019 • Accepted: 9 September 2019 •
Published Online: XX XX XXXX

View Online Export Citation CrossMark

Quentin Galand,[1,a)] Stéfan Van Vaerenbergh,[1] Werner Köhler,[2] Oleg Khlybov,[3] Tatyana Lyubimova,[3] Aliaksandr Mialdun,[1] Ilya Ryzhkov,[4,5] Valentina Shevtsova,[1] and Thomas Triller[2]

AFFILIATIONS

[1]MRC, Université libre de Bruxelles, Department of Chemical Physics, Avenue F. D. Roosevelt, CP165/32, B-1050 Brussels, Belgium
[2]Physikalisches Institut, Universität Bayreuth, 95440 Bayreuth, Germany
[3]Institute of Continuous Media Mechanics UB RAS, Koroleva, 1, 614013 Perm, Russia
[4]Institute of Computational Modelling SB RAS, 660036 Krasnoyarsk, Russia
[5]Siberian Federal University, Svobodny 79, 660041 Krasnoyarsk, Russia

[a)]**E-mail:** qgaland@ulb.ac.be. **Tel.:** (+32)26506576. **Fax:** (+32)26503126.

ABSTRACT

The Soret coefficients of a set of ternary systems of 1,2,3,4-tetrahydronaphthalene (THN), isobutylbenzene (IBB), and n-dodecane (nC_{12}) at 298.15 K were measured under microgravity condition aboard the International Space Station in the frame of the DCMIX1 experiment. The present work includes a comprehensive study of possible data processing sequences for the interpretation of interferometric Soret experiments in ternary systems. Several data processing methodologies are discussed. A significant concentration dependence of the Soret coefficients is observed. In the present study, we have obtained large and positive values for THN and negative ones for IBB in all investigated systems. A linear relation between the Soret coefficients of two components is derived for each system and allows validating experimentally the coefficients measured in other experiments.

I. INTRODUCTION

The study of thermodiffusion in multicomponent systems raises a great level of interest in the scientific community. Molecular diffusion and thermodiffusion play an important role in many natural[1,2] and industrial[3] processes and for the fundamental understanding of the behavior of liquid mixtures.[4–6] Thermodiffusion, or the Soret effect,[7] refers to a species transfer mechanism due to a local temperature gradient. The experimental techniques for the measurement of Soret coefficients in binary mixtures are well known and were presented in several reviews.[8–11] In recent years, a large amount of experimental work was devoted to the study of the Soret effect in multicomponent systems.[12]

In the present paper, we provide the Soret coefficients obtained from the measurements performed in ternary liquid systems aboard the International Space Station (ISS) during the DCMIX1 (Diffusion Coefficient Measurements in mIXtures) experiment. DCMIX1 is part of the DCMIX program that is endorsed by the European Space Agency and includes four experiments, studying several ternary liquid systems. During the DCMIX1 measurement campaign, a series of experimental runs were performed, studying ternary mixtures composed of 1,2,3,4-tetrahydronaphthalene (THN), isobutylbenzene (IBB), and n-dodecane (nC_{12}) with different concentrations at 25 °C. The experimental conditions are such that species transport results from the combined effect of thermal gradient and molecular diffusion. In a ternary system, the diffusive flux J_i of component i

can be written as[13]

$$J_i = -\rho \sum_{j=1}^{2} D_{ij} \nabla w_j - \rho D'_{T,i} \nabla T, \quad (1)$$

where ρ is the density of the liquid, D_{ij} are the molecular diffusion coefficients, w_i and $D'_{T,i}$ are, respectively, the mass fraction and thermodiffusion coefficient of component i, and T is the temperature.

Significant data analysis and processing work is required in order to retrieve accurate values for the Soret coefficients. The raw data were simultaneously analyzed by several research teams and compared prior to publication. In the present paper, we detail the experimental setup and procedure, compare the different data processing methodologies, and report and discuss the obtained Soret coefficients.

II. EXPERIMENTAL

In this section, we discuss several aspects of the experiments. First, we explain the principle of the experimental technique in Sec. II A. The choice of the studied systems, the experimental setup, and the experimental procedures are described in Sec. II B.

A. DCMIX experiment

The principle of the DCMIX experiment was proposed in Ref. 14 for the experimental determination of the diffusion coefficients of liquid mixtures. The concentration gradient used to observe molecular diffusion is created through the Soret effect by placing the liquid in a nonuniform temperature field. This idea was already used in a number of previous studies, such as the laser beam deflection technique by Kolodner in 1987,[15] but here the chemical composition field is observed by the means of an interferometric technique. Modern interferometric techniques allow obtaining a map of the chemical composition in liquid systems with a high spatial and temporal resolution. The Selectable Optical Diagnostic Instrument (SODI) allows obtaining in one single experiment both the Soret and the diffusion coefficients. In this paper, the study is limited to the determination of the Soret coefficients only.

The experiment starts with a homogeneous system at constant temperature; at the beginning of the "*Soret step*" of a run, a temperature gradient is created in the liquid by placing the bottom and top walls of the liquid volume at two different temperatures. The temperature gradient is kept constant, and thermodiffusion induces the migration of the components. Once the system has reached a steady state, in a closed cell, with no convection and no chemical reaction, the diffusion fluxes vanish and the composition gradient along the cell is proportional to the temperature gradient. From Eq. (1), this can be written as

$$\nabla w_i = -S'_{T,i} \nabla T, \quad (2)$$

where we introduced the modified Soret coefficients $S'_{T,i}$. 99% of the separation is obtained after about five times the characteristic diffusion time. In ternary systems, characteristic diffusion time $\tau = L^2/(\pi^2 D_s)$ can be computed using the cell height L and the smaller eigenvalue D_s of the diffusion matrix.[16] This corresponds to the end of the *Soret step* of the runs in on-board operations. The so-obtained concentration differences Δw_i of the components across the cell provide the Soret coefficients by the relation

$$\Delta w_i = -S'_{T,i} \Delta T, \quad (3)$$

where the differences Δ are from the top wall with respect to the bottom wall of the cell. After the *Soret step*, the temperature gradient is removed; the "*Diffusion step*" then develops and Eq. (1) applies with a vanishing temperature gradient,

$$J_i = -\rho \sum_{j=1}^{2} D_{ij} \nabla w_j. \quad (4)$$

The typical timeline of an experimental run is shown schematically in Fig. 1.

B. Experimental

The primary objective of the DCMIX1 experiment is to obtain accurate and reliable experimental data about the diffusive properties of multicomponent systems, in a convection free environment. The project originated from the collaboration between several academic research centers with partners from the oil industry during which binary, ternary, and quaternary Soret coefficients were obtained in microgravity conditions in the SCCO experiment.[17–19] Three chemical species were selected to represent three major families of compounds found in crude oils: THN, IBB, and nC_{12}, respectively, for the families of naphthenic, aromatic, and aliphatic compounds. The selected systems involve three components and are away from the dilution limits. Nondiluted ternary systems carry the main aspects of multicomponent systems, and chemo-diffusive couplings specific to multicomponent systems appear as soon as more than two nondiluted components are diffusing. The concentrations of the systems investigated in DCMIX1 are summarized in Table I.

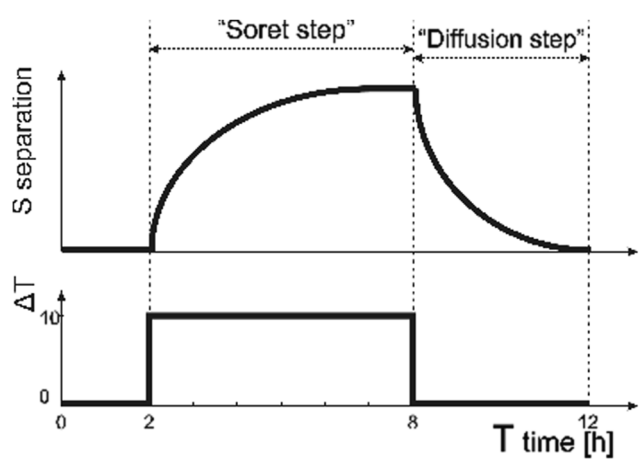

FIG. 1. Principle of an interferometric Soret diffusion experiment. Prior to the experiment, during the thermalization phase, the entire cell is kept at constant temperature. During the "Soret step," a temperature gradient is applied to the liquid and the Soret effect induces a gradient of the chemical components in the system. During the "Diffusion step," the temperature gradient is removed and the diffusion coefficients are quantified by observing the relaxation of the liquid induced by molecular diffusion.

TABLE I. Concentrations of the systems investigated in the DCMIX1 experiment.

Cell	Component mass fraction (%) THN	IBB	nC_{12}	Experimental runs processed in this study
0	50	...	50	NA
1	10	10	80	16, 21
2	10	80	10	2^E, 07, 17, 22, 27
3	80	10	10	See Ref. 12
4	45	10	45	4^E, 19, 24
5	40	20	40	5^E, 15, 20, 25

In Fig. 2, the mixtures investigated in DCMIX1 are shown with red points. Five primary cells, cells 1–5, were filled with ternary mixtures, and one companion cell, cell 0, was used to study a binary system with equal mass factions of *THN* and nC_{12}. The compositions are such that points are aligned in the ternary concentration diagram, with the aim of investigating mixing rules.[17,20–23]

The diffusion and Soret coefficients of the corresponding binary systems have been measured by several experimental techniques in the frame of the Fontainebleau benchmark,[24,25] and the ternary diffusion coefficients were recently measured on ground.[12,16,26,27] For each system investigated during the DCMIX1 campaign aboard the ISS, several experimental runs were performed. For cell 1, liquid leaked out of the cell during the measurement campaign. A bubble appeared in the cell, and only two experimental runs were completed.

For each cell, two different durations of the runs were used. In addition to the "standard runs," "extended runs," denoted with superscript *E* in tables Table I, have been proposed in the event that the diffusion coefficients of one investigated system are significantly lower than foreseen.

Each run starts with a thermalization phase during which the temperature of the cell is stabilized to 25 °C. The top and bottom cell walls are then brought to 20 and 30 °C, respectively. A stationary temperature gradient quickly establishes in the liquid, and the thermodiffusion process is monitored during a given time. The temperature gradient is then removed, and isothermal diffusion is observed. The duration of the "*Soret step*" was selected so that the Soret separation attains the steady state. The duration of the "*diffusion step*" was chosen to cover several characteristic molecular diffusion times.

For some runs, data are acquired simultaneously for the companion cell and for a primary cell. The measurements in the companion cell are carried out in order to study the possible influence of the residual gravity on the experiments, a topic of interest for microgravity assessment,[28–31,57] and to cross-check with ground based measurements.

The liquid is placed in a parallelepipedic cell, as shown in Fig. 3. The four lateral sides of the cell are transparent, allowing optical probing. The temperatures of the upper and lower metallic walls of the cell are controlled precisely and independently by Peltier modules. During the DCMIX1 measurement campaign, the six systems presented in Table I are arranged in a cell array and studied sequentially.[32] Details regarding the cell design can be found in Ref. 26.

The chemical composition within the binary system of the companion cell is visualized with a standard Mach-Zehnder type interferometer. A movable two-wavelength interferometer, which can be moved to the selected cell, probes the primary cells.[33] The wavelengths of the laser diodes used are λ_1 = 670 nm and λ_2 = 935 nm.

The components of the experimental setup were assembled inside the US Destiny module where ISS residual gravity is lowest. A set of parameters monitoring the functioning of the experiment are both simultaneously displayed in real time on ground and stored

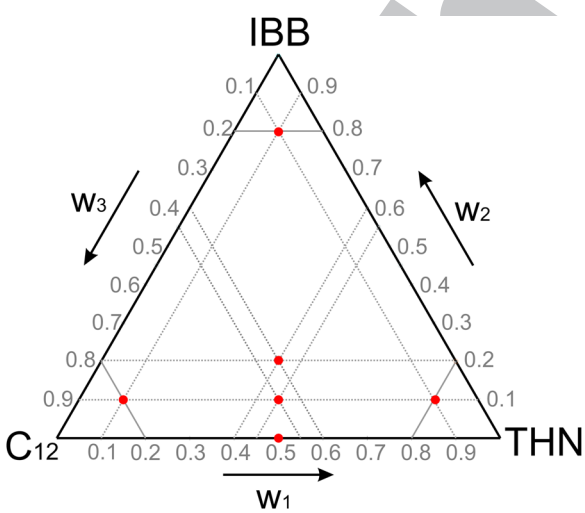

FIG. 2. Concentrations of the systems investigated in DCMIX1. The concentrations of the systems investigated under microgravity conditions in DCMIX1 are shown by red dots in a ternary diagram. Systems characterized by aligned points in the diagram were selected for the investigation of mixing rules.

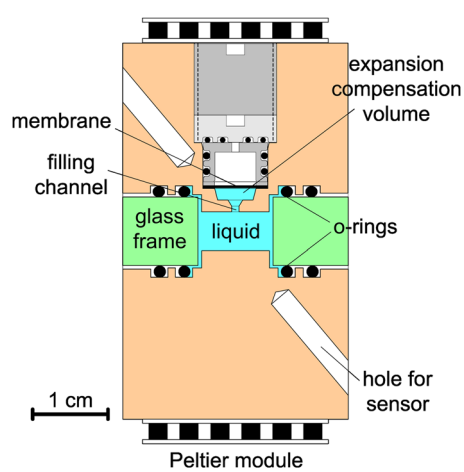

FIG. 3. Schematic of a DCMIX experimental cell. The liquid volume is sealed by O-rings. Two Peltier elements are used to control the temperatures of copper parts. Temperature sensors probe the temperatures of the copper parts.

on flash disks. The data were distributed to the science team by the MARS center.[34]

III. DATA PROCESSING

The data obtained from the experiment are a set of digitized interferograms. The data processing methodology implemented to obtain the Soret coefficients from the experimental data consists of a sequence of five main steps. As discussed in Ref. 35, for each step, several possibilities can be envisaged; this results in a wide variety of data processing approaches, as shown diagrammatically in Fig. 4. During the course of previous benchmarking for DCMIX1,[12] several teams have processed the same set of experimental data by different processing schemes. The mass transfer coefficients, obtained by different procedures, have revealed large dispersion. To address this problem, in the present study, we investigate 7 data processing schemes, referred to as DP 1–7 in Table II, and we compare in detail the transport coefficients obtained.

The different possible implementations of the 5 steps of Fig. 4 are discussed in the following.

The capital letters A to E refer to the major successive steps of the data processing sequence. The possible implementations of each step are indicated by numbered panels.

A. Input experimental data

The first step of the data processing scheme is the selection of the experimental data used for the estimation of the transport coefficients. In Table II, data processing schemes 1–4 analyze the data collected during the *Soret phase* of an experimental run, while data processing schemes 5–7 use the data corresponding to the *diffusion phase* of the runs.

TABLE II. Data processing sequences used in the present study.

DP	Processing sequence	Authors
1	A1 B1 C1 D3 E3+4	AM, VS (ULB)
2	A1 B1 C1 D3 E2+3	AM, VS (ULB)
3	A1 B1 C3 D3 E4	TT, WK (UB)
4	A1 B2 C1 D4 E3+4	OK, IR, TL (RAS)
5	A2 B2 C1 D4 E3+4	OK, IR, TL (RAS)
6	A2 B1 C3 D2 E4	QG, SVV (ULB)
7	A2 B1 C1 D1 E4	QG, SVV (ULB)

In optical probing, the spatial concentration variation in the liquid is evaluated by measuring changes in the refractive index. During the Soret step of the experimental runs, the refractive index n of the ternary system varies with its temperature and with its chemical composition,

$$\Delta n_i = \frac{\partial n_i}{\partial T}\Big|_{w_1,w_2}\Delta T + \frac{\partial n_i}{\partial w_1}\Big|_{w_2,T}\Delta w_1 + \frac{\partial n_i}{\partial w_2}\Big|_{w_1,T}\Delta w_2, \qquad (5)$$

where the symbol Δ here denotes the changes of quantities with respect to their equilibrium values. The thermal and molecular diffusivities differ by about two orders of magnitude, and it is easy to separate the two last terms on the right hand side (RHS) of Eq. (5) from the thermal signal contribution. The thermal field is obtained from the early images of the *Soret step* of the runs, while the images recorded later are used to obtain the concentration changes Δw_1 and Δw_2. During the diffusion step of the experiments, the liquid is isothermal and the first term on the RHS of Eq. (5) vanishes. The fringe density significantly increases when the temperature gradient

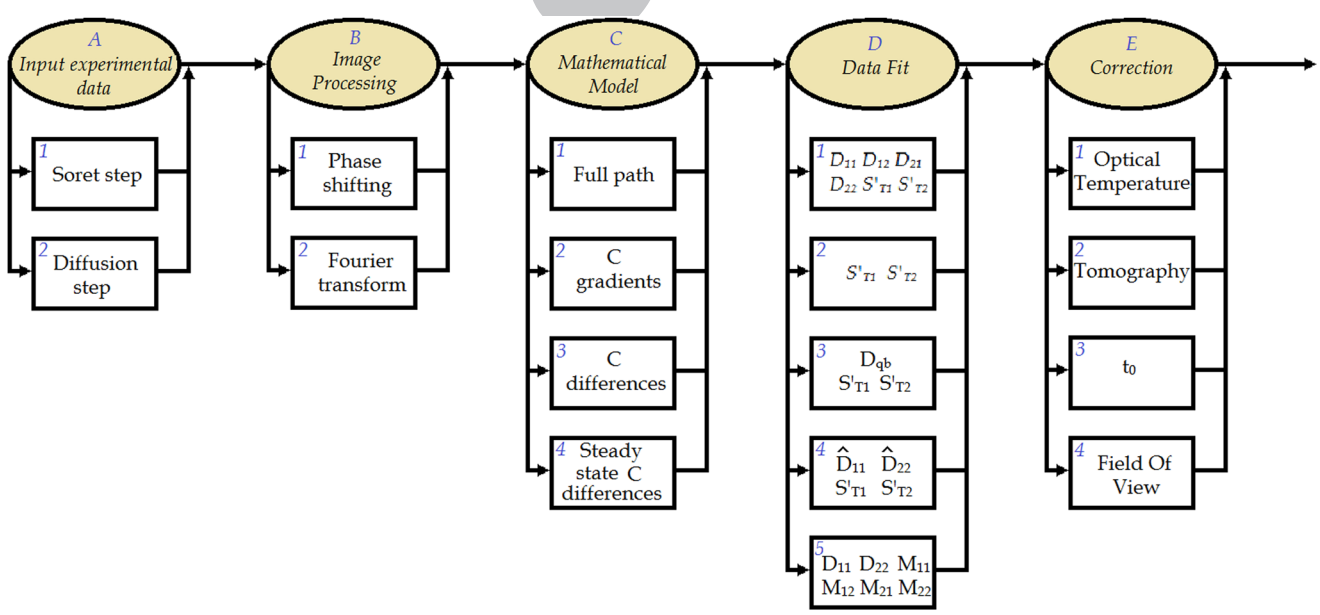

FIG. 4. Simplified diagram of possible schemes for processing interferometric Soret-diffusion experimental data. The top panels A to E indicate the major successive steps. The possible implementations of each step are indicated by numbered panels.

is imposed across the cell, as easily observed from two experimental images shown in Fig. 5.

B. Image processing

By design, the interpretation of interferometric experimental data requires the use of a 5 step image processing method. Before the image processing procedure, the images are cropped and rotated to exclude the regions outside the sample volume and to align the plates of the cell horizontally. The first step, the phase calculation, is the determination, directly from the interferograms, of a wrapped phase change Ψ. In the second step, a reference image is subtracted from every image since the individual phase values are meaningful only when compared to a reference state. $\Delta\Psi$ is wrapped into the interval $[-\pi, \pi]$. The third step, phase unwrapping, allows obtaining the phase change $\Delta\varphi$ of the light of wavelength λ traversing the sample along the geometrical path e that results from a refractive index change Δn,

$$\Delta\varphi = \frac{2\pi e}{\lambda}\Delta n. \tag{6}$$

Finally, the unwrapped phase is converted into the refractive index using Eq. (6).

1. Phase calculation

The image acquisition technique used is a phase shifting interferometry.[36,37] It consists in acquiring several fringe images that are phase shifted by an integer fraction of 2π of the object and calculating the resulting phase signal with a phase shifting algorithm. In SODI, phase shifts are obtained by stepping the laser diode currents. For DCMIX1, the selected technique is based on the acquisition of a set of five fringe images with a phase shift of $\pi/2$. The acquisition of five images is achieved within less than a second, a time where the refractive index field can be considered constant. This assumption is perfectly reasonable since the characteristic time of the experiments is of the order of several hours. In the data processing schemes DP 1 and 2 of Table II, phase images were computed using the Hariharan algorithm.[38] In DP3, a modified[39] version of the Hariharan equation was implemented.[40] In DP 4 and 5, the widely known Fourier filtering method[41,42] was applied. This method allows reconstructing the optical phase from a single interference image. A detailed description of the method is provided in Refs. 33 and 43. As discussed in Ref. 38, for many DCMIX images, significant phase shift errors were observed, resulting in strong disturbances of the phase signal when standard stepping algorithms are straightforwardly applied. In DP 6 and 7, to address this problem, the phase signals were recovered with iterative algorithms.[44] All the above-mentioned methods differ substantially in their basic principles; therefore, one can expect some differences between the obtained signals. Note that even within the same methodology, difference in results obtained by different researchers may arise due to the implementation of the algorithms.

2. Reference subtraction

Interferometry, by principle, is a differential measuring technique: the measured quantity is the variation of the refractive index field with respect to a reference, commonly referred to as the "reference image." When processing the images acquired during the Soret phase of the runs, the reference image corresponds to the beginning of the Soret phase, right after the establishment of the temperature gradient in the liquid, so that the reference subtraction allows separating the thermal and compositional parts of the experimental signals of Eq. (5). On the other hand, when performing the processing of the images of the *diffusion phase* of the runs, the reference image is acquired at the end of the thermalization phase of the runs, prior to the *Soret phase*.

3. Phase unwrapping

Phase unwrapping is a well-known problem in interferometry, and many different algorithms have been proposed to remove the phase ambiguity.[45] In DP1, DP2, and DP3, a modified[40] version of the Itoh algorithm[46] was implemented; in DP 4 and 5, the wrapped phase images are of sufficient quality, the phase exhibit a strict horizontal alignment, and a one-dimensional sequential phase unwrapper was employed;[33] in DP6 and 7, the Costantini[47] algorithm was used.[48]

4. Contrast factors

These image processing operations are performed independently for the two sets of images acquired for the two wavelengths of the two-color interferometer and allow obtaining two series of refractive index maps $\Delta n_i(x, y, t)$. The concentration fields are then obtained with the following equation:

$$\begin{pmatrix}\Delta w_1\\ \Delta w_2\end{pmatrix} = \begin{pmatrix} n_{1,1}|_2 & n_{1,2}|_1\\ n_{2,1}|_2 & n_{2,2}|_1\end{pmatrix}^{-1}\begin{pmatrix}\Delta n_1\\ \Delta n_2\end{pmatrix}, \tag{7}$$

where we introduced the optical contrast factors $n_{i,j}|_k$, defined as

$$n_{i,j}|_k = \frac{\partial n_i}{\partial w_j}\Big|_{T,P,w_{k,k\neq j}}. \tag{8}$$

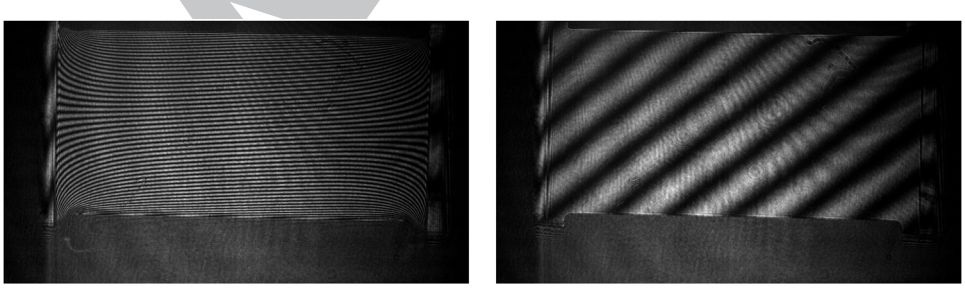

FIG. 5. Comparison of typical interference patterns. Left: pattern recorded during the Soret phase of an experimental run. Right: pattern recorded during the diffusion phase.

TABLE III. Contrast factors for the 5 ternary systems studied in the DCMIX1 experiment at T = 25 °C. Component 1 is *THN*, component 2 is *IBB*, and component 3 is nC12. Contrast factors are defined in Eq. (8). Those values were computed from Ref. 49.

Cell	w_1	w_2	w_3	$n_{1,1}\|_2$	$n_{1,2}\|_1$	$n_{2,1}\|_2$	$n_{2,2}\|_1$	K
1	10	10	80	0.0960	0.0547	0.0926	0.0521	342
2	10	80	10	0.1248	0.0758	0.1198	0.0714	254
3	80	10	10	0.1427	0.0887	0.1374	0.0838	241
4	45	10	45	0.1149	0.0686	0.1107	0.0655	495
5	40	20	40	0.1164	0.0696	0.1120	0.0667	1092

The contrast factors are experimentally measured in ground experiments. The computed values of the Soret coefficients strongly depend on the values of the contrast factors used for the calculations. In the present study, all teams used identical contrast factors, computed using the methodology and the experimental data reported in Ref. 49 and summarized in Table III.

An algorithm for identification of the transport coefficients requires the inversion of the matrix of optical contrast that can be ill conditioned.[49] The conditioning of a matrix is characterized by a condition number K.[35] The smaller the condition number, the lower the error amplification when computing the concentration of the components from the interferograms.

C. Data fitting

Identification of the mass transport coefficients is performed by fitting the analytical solution of Eq. (1) to the experimental data extracted from the processed images. The concentration distribution can be written in different ways. The most widely used analytical solutions are the full path solution[26,35,43,51] that includes all available data points, both in time and in space; the gradient solution,[33,35,52] similar to the optical beam deflection (OBD) approach,[53] which describes the gradient of concentration at midheight of the cell; and the concentration difference solution,[32,54] which describes the temporal evolution of the difference of concentration between the top and the bottom of the cell. Each of the above provides both Soret and diffusion coefficients, but the amount of data involved in the identification of the mass transport coefficients is essentially different and the use of the different approaches can lead to slightly different results. Finally, one can simply analyze the concentration gradient at steady state by processing the image obtained at the end of the Soret phase of the run (or alternatively at the beginning of the diffusion phase, as proposed in Ref. 48). This method allows retrieving the Soret coefficients directly with Eq. (2) and does not require identifying the diffusion coefficients. As can be seen from Fig. 6, the two phase signals obtained at different wavelengths are clearly separated from each other.

In general, the mathematical solution of a Soret diffusion experiment in ternary mixture comprises six unknowns, four diffusion coefficients D_{11}, D_{12}, D_{21}, and D_{22}, and two Soret coefficients $S'_{T,1}$ and $S'_{T,2}$. To obtain reliable fitting results, different strategies were tested in this study. In the first, as done in DP 7, the six unknowns are fitted directly. This technique, however, provides diffusion coefficients that are very sensitive to noise. Using specific combinations of unknown quantities in the analytical solutions, the problem can

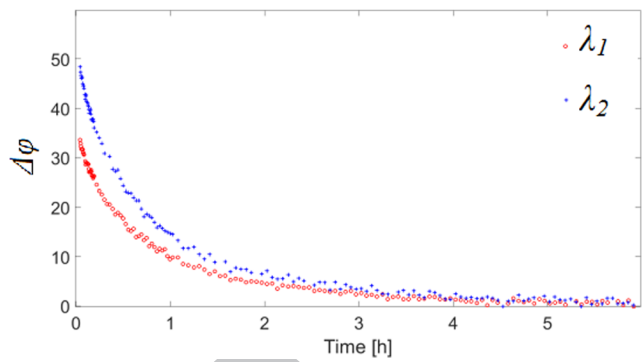

FIG. 6. Typical phase signals obtained after image processing of the data of a DCMIX1 experimental run. The two optical signals, corresponding to the two wavelengths of the two-color interferometer, λ_1 = 670 nm, λ_2 = 935 nm, are of similar shape but different amplitude.

be converted to four parameters[33] (two Soret coefficients and two diffusion eigenvalues, $\widehat{D}_1$ and $\widehat{D}_2$). The mathematical details of different models are available elsewhere.[35] This methodology was applied in *DP*2 and *DP*3. Moreover, assuming that the two diffusion eigenvalues are equal,

$$\widehat{D}_1 = \widehat{D}_2 = D_{qb}, \tag{9}$$

meaning that ternary diffusion can be modeled as quasibinary diffusion, the problem is then simplified to a three-parameter fit.[26] This methodology was used in DP1 and DP2. In DP3 to DP5, the mathematical modeling requires defining an amplitude matrix $\boldsymbol{M}$.[27,52] The fitting identifies 6 unknowns, the four elements of $\boldsymbol{M}$ and the two diffusion eigenvalues. Alternatively, in the steady state concentration gradients method, used in DP6, only the two Soret coefficients are fitted.[48]

We want to emphasize that for the present work, the shapes of the transients and, hence, the diffusion eigenvalues, were not analyzed in full detail since they are irrelevant for the asymptotic amplitudes that determine the Soret coefficients. This becomes most apparent in the quasibinary approximation of Eq. (9), where the two eigenvalues are even set equal. The diffusion eigenvalues of the systems were measured elsewhere, by the Taylor Dispersion Technique (TDT),[16] by the Optical Beam Deflection (OBD),[52] and by the Sliding Symmetric Tubes (SST).[55] Additional experimental data obtained by the SST[56] and by the open ended capillary method[48] were also reported for cell 3 in the frame of a benchmark.[12] Those data are summarized in Table IV.

D. Corrections

Due to the DCMIX cell design, the temperature field in the liquid is not perfectly linear. As a consequence, see Eq. (1), the concentration distribution, and therefore the measured refractive index fields, is also not linear. However, the working equations describing the problem apply linear concentration profiles. As a consequence, optical integration of the deformed refractive index fields leads to underestimated values of the Soret separation. Different suggestions for the correction of the data were proposed. In Ref. 32, the authors use a so-called "*optical temperature*" (see Sec. IV A) in Eq. (3) to

Q4

TABLE IV. Diffusion eigenvalues and mean eigenvalue $\bar{D}$ for the DCMIX1 systems. Those values were obtained by the Taylor Dispersion Technique (TDT) in Ref. 16, by the optical beam deflection in Ref. 52, by the Sliding Symmetric Tubes (SST) in Refs. 55 and 56, and by the open ended Capillary in Ref. 48.

C	Reference	$\hat{D}_1$ (10^{-10} m^2 s^{-1})	$\hat{D}_2$ (10^{-10} m^2 s^{-1})	$\bar{D}$ (10^{-10} m^2 s^{-1})
1	TDT[16]	11.9	8.8	10.35
	OBD[52]			6.02
	SST[55]	11	9	10
2	TDT[16]	10.9	9	9.95
	OBD[52]			9.82
	SST[55]	12	9	10.5
3	Benchmark[12]	6.61	5.48	6.04
	TDT[16]	7.4	5.3	6.35
	OBD[52]			9.29
	OEC[48]	6.60	5.50	6.05
	SST[65]	8.08	5.43	6.75
4	TDT[16]	8.5	6.2	7.35
	OBD[52]			6.65
	SST[55]	7	7	7
5	TDT[16]	8.9	6.5	7.7
	OBD[52]			7.03
	SST[55]	7	4	5.5

compute the Soret coefficients. In the present study, all the Soret coefficients were computed with a temperature difference of 10 °C, as measured by the temperature sensors. In Refs. 26, 35, 57, and 58, the authors recommend performing a tomography reconstruction of the concentration profiles in the center of the cell to account for the curvature of the temperature field. This approach is used in DP2 in our study.

Q5 At short times, both in the Soret and the diffusion phase of the runs, the hypothesis of the temporal separation of the thermal and compositional transients is not strictly valid.[50] During the temperature transient, diffusive concentration changes do happen close to the top and bottom walls of the cell,[59] but are not observed in the interferograms, due to the reference image subtraction. In DP1, DP2, DP4, and DP5, this effect is taken into account by introducing an additional fitting variable, an initial time t_0, as discussed in Refs. 26, 33, and 43.

The temperature field in the cell is more linear in the central part, and more curved in the external regions of the cell, approaching the upper and lower heating elements or the Quartz walls. DP 4, DP5, DP6, and DP7 only take into account a limited central region of the field of view of the interferograms.

IV. RESULTS AND DISCUSSION

A. Thermal analysis

The thermal regulation timeline of the cells includes several steps. We present in the following figures the typical evolution of the temperatures T_1 and T_2 in the top and bottom part of each experimental cell. For all the runs for cells 0–4, the performance of the temperature regulation was very similar. A typical plot of the temperatures T_1 and T_2 for those runs is showed in Fig. 7.

In Fig. 7, the speed of the regulation during the buildup and the removal of the temperature gradient are illustrated by temporal zooms. For all the runs, 90% of the temperature gradient is established or removed within a little less than 1 min and more than 99% is stabilized within 2 min. The third zoom shows that the temperature regulation is stable and precise: during the *Soret step*, the maximum deviation between the measured and set point temperatures is 0.02 °C; during the *diffusion step*, it is 0.05 °C. Similar temperature profiles were observed for all runs for cells 0–4. For all runs on cell 5 however, notable deviations from the nominal temperatures were observed throughout the experiments, as depicted in Fig. 8. The cause of the occasional malfunction of the temperature regulation for this cell could not be revealed.

For those runs, numerous temperature spikes were detected, during which the difference between the set-point and measured temperatures was of the order of 0.2–0.4 °C.

As mentioned earlier, the characteristic heat and mass diffusion times differ by about two orders of magnitude. The analysis of the interferometric data at the beginning of the *Soret step* allows obtaining information about the temperature field across the cell. We report here the data obtained for the binary system, referred to as cell 0 in Table I. Both temperatures were stabilized at 25 °C before acquiring a reference image. T_1 was then raised to 30.00 °C,

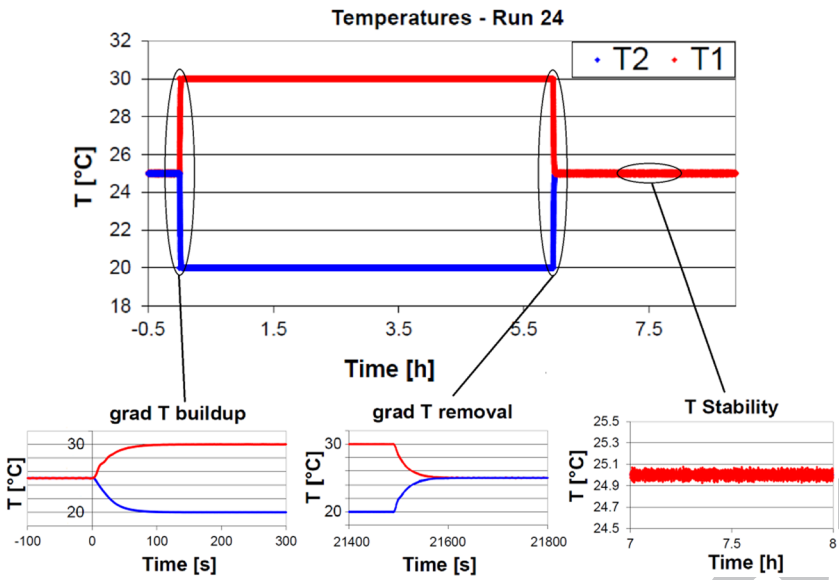

FIG. 7. Typical temperature cycle performed in a DCMIX1 run for cells 0–4. In the bottom of the figure, several zooms are shown to illustrate the performances of the temperature regulations.

while T_2 was cooled down to 20.00 °C. 2 min later, a second interferometric image was acquired. This corresponds to more than 5 times the characteristic heat diffusion time for the investigated liquids. The corresponding phase images were calculated and processed as described in Fig. 9. The observed phase change is shown in Fig. 10.

A map of the refractive index change was calculated with Eq. (10). Interferometry measures the average refractive index change across the liquid sample (here, average means integrated along the optical axis of the interferometer). It is then possible to determine a 2D map of the average temperature in the liquid, the "optical temperature" T_{opt},

$$T_{opt} = \frac{\Delta n_1}{n_{1,T}}, \tag{10}$$

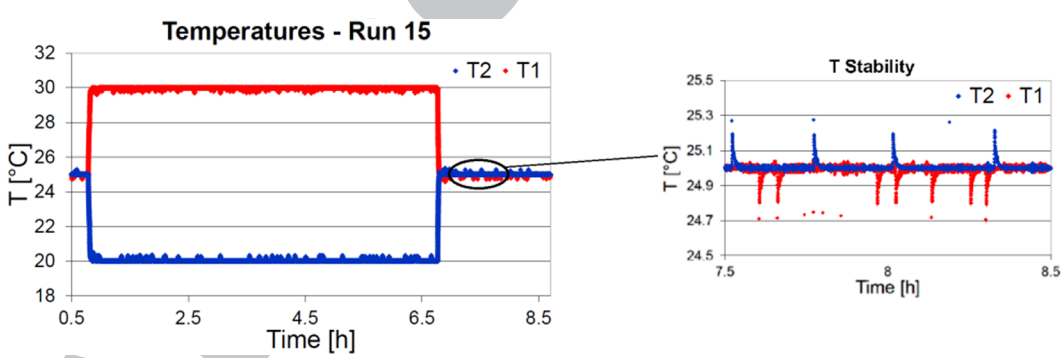

FIG. 8. Typical temperature cycle performed in a DCMIX1 run for cell 5. These measurements show that temperature control did not function nominally for cell 5. Notable deviations from the nominal temperatures were observed. The cause of the malfunction could not be revealed.

Q6

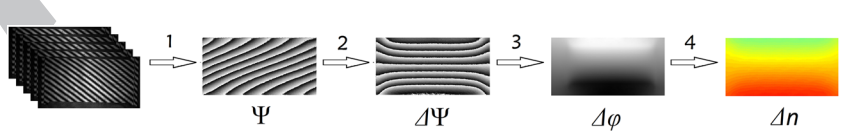

FIG. 9. Image processing steps for the translation of interferometric experimental of a Soret diffusion experiment. Step 1 is phase calculation, step 2 is reference image subtraction, step 3 is phase unwrapping, and step 4 is computation of refractive from the unwrapped phase.

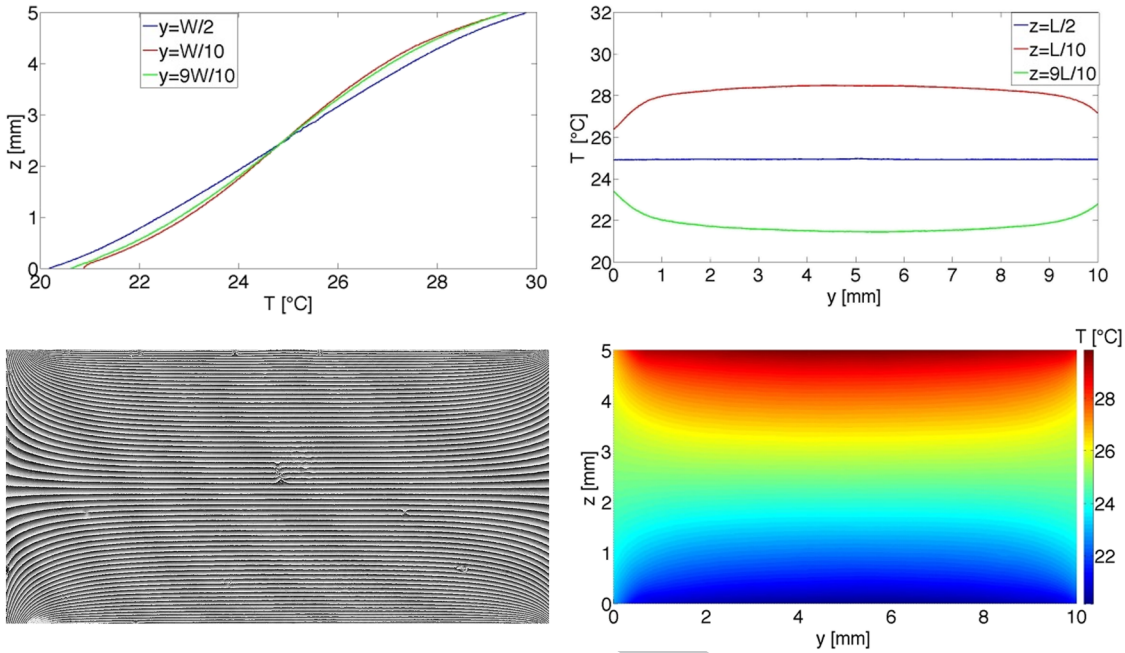

FIG. 10. Temperature field in cell 0. Top left: phase map recorded right after the establishment of a stationary temperature field in the cell. Top right: colormap of the computed temperature in the liquid. Bottom left: vertical temperature profiles in the liquid. Bottom right: horizontal temperature profiles in the liquid. Q7

where $n_{1,T} = \partial n_1/\partial T|_{w1,w2} = -0.004\,47$ is the thermal contrast factor at wavelength λ_1.[60] In Fig. 10, we observe a strong curvature of the temperature field approaching the edges of the cell. The temperature difference between the top and the bottom of the cell is close to 10 °C in the center of the cell but significantly smaller at the Quartz walls. The temperature profiles along several vertical and horizontal lines are plotted in Fig. 10.

B. Soret coefficients

The refractive index difference between the top and the bottom of the cell $(n_{tb})_i$ for both wavelengths and the corresponding Soret coefficients obtained by using the 7 different data processing schemes are reported in Table V. We do not report data for cell 3 in the present paper, as it was previously studied in detail.[12,26,32,33,48,54]

In Table V, outlier data points corresponding to $S'_{T,1}$ or $S'_{T,2}$ and deviating of more than 2 standard deviations from the mean coefficients are indicated by a * superscript. Based on this set of results, we report in Table VI the mean Soret coefficients obtained in the present study, together with the coefficients found in the literature, including coefficients obtained by OBD,[52] by a previous analysis of DCMIX1 data[32,54] and by combination of SST and thermogravitational column experiments (SST + TC).[55] Q8

For cells 1–4, at least 2 Soret coefficients were obtained with a reasonable accuracy. For cell 5, the experimental data did not allow identifying accurately the Soret coefficients. We provide the coefficients obtained for cell 5, but we acknowledge that given the amplitude of the standard deviation, these values should be taken with caution. The first observation is that, in all systems, the heavier component, tetralin, showed a positive Soret effect, which means that it concentrated at the cold side of the cell. Moreover, the magnitude of the separation of tetralin is larger than that of the two other components (except in cell 5). The systems studied through the first three cells are located close to the three corners of the ternary concentration diagram (see Table I), where one of the components is more concentrated than the other two (nC_{12} in cell 1, *IBB* in cell 2, and *THN* in cell 3). The comparison of the results obtained for these cells provides an illustration of the complexity of thermodiffusion in multicomponent mixtures. We do not observe any obvious correlation between the concentration of the components and the amplitude of the Soret coefficients. In the present study, we obtained a negative coefficient for IBB, but this observation is not confirmed by previous experimental studies. In cell 2, $S'_{T,2}$ is larger than $S'_{T,3}$, while in cells 1 and 3, $S'_{T,3}$ is larger. The separation of tetralin is significantly larger in cells 4 and 5 than in cells 1–3.

1. Comparison of data processing approaches

As indicated in Eq. (2), the steady state thermodiffusive concentration fields are proportional to the temperature field in the cells. Due to the curvature of the temperature field, the refractive index differences measured by interferometry tend to underestimate the Soret separation. Data processing sequences DP1 and DP2 used identical image processing algorithms and mathematical models, the only difference being the tomographic reconstruction of the refractive index fields. Thus, the refractive index differences, and the Soret coefficients, computed by DP2 are significantly larger than the ones obtained by DP1.

TABLE V. Refractive index differences at both wavelengths and Soret coefficients obtained with the 7 data processing sequences of Table II. Components 1, 2, and 3 are, respectively, *THN*, *IBB*, and nC_{12}; C is the cell number; DP is the data processing scheme according to Table II; and run is the run reference according to Table I. * superscript denotes outlier data points.

C	DP	Run	$-(n_{tb})_1$	$-(n_{tb})_2$	$S_T'{}_1$	$S_T'{}_2$
			10^{-4}		10^{-4} K^{-1}	
1	1	16	6.103	5.929	9.41	−5.35
		21	6.086	5.921	10.07	−6.53
	2	16	6.852	6.662	11.04	−6.76
		21	6.836	6.645	10.85	−6.54
	3	16	6.107	5.952	11.0	−8.1
		21	6.119	5.946	9.5	−5.5
	4	16	5.78	5.73	*18.8	*−2.24
		21	5.77	5.69	*15.8	*−17.1
	5	16	6.22	6.07	12.2	−10.0
		21	6.26	5.98	*1.0	*9.7
	6	11	6.161	5.924	4.61	3.17
		16	5.790	5.630	9.33	−5.79
		21	5.710	5.520	6.64	−1.21
	7	16	6.314	6.065	4.2	4.17
		21	6.181	5.947	4.9	2.7
2	1	17	5.133	4.978	6.55	−4.01
		02	5.199	5.041	6.58	−3.98
		22	5.148	5.004	7.11	−4.91
		27	5.172	5.023	6.93	−4.60
		07r	5.202	5.042	6.50	−3.83
	2	17	5.714	5.545	7.45	−4.73
		02	5.757	5.578	7.09	−4.09
		22	5.730	5.564	7.63	−5.00
		27	5.742	5.578	7.76	−5.20
		07r	5.780	5.622	8.14	−5.78
	3	2	5.2428	5.087	6.8	−4.3
		17	5.2307	5.063	6.2	−3.3
		22	5.2122	5.062	7.0	−4.6
		27	5.2272	5.073	6.9	−4.4
	4	2	5.04	4.87	5.9	−3.0
		17	4.92	4.84	9.3	−8.9
		22	4.97	4.82	6.3	−3.8
		27	4.96	4.84	7.6	−5.9
		27 r	4.93	4.85	*9.8	*−9.6
	5	2	5.06	4.81	*2.1	*3.3
		17	−5.01	−4.79	*2.7	*2.2
		22	−4.99	−4.81	4.8	−1.3
		27	−4.99	−4.78	3.4	0.9
		27r	4.98	4.86	7.8	−6.3
	6	2	5.613	5.416	6.0	−2.4
		12	5.359	5.192	6.08	−3.0
		17	5.359	5.192	6.59	−3.78
	7	2	5.286	5.092	5.09	−1.41
		7	5.251	5.063	5.31	−1.82
		12	5.172	5.067	9.00	−8
		22	5.241	5.067	5.91	−2.82
4	3	4	21.022	20.431	34.9	−27.8
		19	20.898	20.312	34.8	−27.8
		24	20.845	20.248	33.4	−25.6
	6	4	20.719	20.063	27.39	−15.68
		19	19.9621	19.3060	24.0	−11.0
		24	19.5198	18.9097	26.6	−16.1
	7	4	20.8220	20.2560	36.79	−31.28
		19	20.6856	20.0665	30.90	−21.60
		24	20.9056	20.3094	34.17	−26.76
5	1	15	18.65	18.10	47.31	−52.29
		20	19.29	18.73	50.84	−57.27
		5	19.13	18.71	79.49	−105.4
		25	18.80	18.25	48.64	−54.30
	2	15	20.96	20.34	55.32	−62.39
		20	22.16	21.52	57.41	−64.18
		5	20.89	20.54	110.44	−54.22
		25	21.23	20.69	70.55	−87.46
	3	5	19.815	19.193	42.2	−42.1
		15	19.105	18.488	37.1	−34.5
		20	19.021	19.169	*200.0	*−308
		25	19.442	18.728	19.2	−4.2
	6	5	*18.27	*17.11	*6.69	*−1.15
		10	19.561	18.915	34.7	−29.9
		15	17.46	17.01	57.9	−71.7
	7	5	18.65	17.93	11.3	7.9
		10	18.5	17.78	8.9	11.7
		15	18.3	17.59	11.0	7.9
		20	18.21	17.49	9.0	11.1
		25	18.48	17.82	23.0	−11.9

DP5 results in the most scattered Soret coefficients. In DP5, the optical phases of the experimental data were collected during the *diffusion step* of the experiments. Due to the alignment of the interferometer in wide fringe configuration, the images collected during this step of the runs only contain a few fringes, and the Fourier algorithm results in noisy phase signals.

DP3 and DP7 are based on very different mathematical modeling of the diffusive processes but implement similar image processing algorithms. The coefficients obtained through these two data processing sequences are very consistent. This seems to indicate that the influence of the image processing algorithms is more critical than the mathematical modeling of the experiments.

TABLE VI. Average Soret coefficients obtained in this study, compared with literature data.[32,52,54,55] Components 1, 2, and 3 are, respectively, *THN*, *IBB*, and nC_{12}. ** superscript denotes corrected data.

C	References	$S_T'{}_1/10^{-4}$ (K^{-1})	$S_T'{}_2/10^{-4}$ (K^{-1})	$S_T'{}_3/10^{-4}$ (K^{-1})
1	This study	8.6 ± 2.8	−3.8 ± 4.8	−4.8 ± 2
	TC + SST[55]	5.4 ± 0.7	3.2	
	OBD[52]	5.8	3.9	−9.0
	DCMIX1[54]	6.02 ± 0.4	−0.42 ± 0.2	
2	This study	6.7 ± 1.2	−4.1 ± 2.0	−2.6 ± 0.8
	DCMIX1[32]	−7.42 (+7.42**)	−0.59 (−5.90**)	
	TC + SST[55]	3.1 ± 0.6	2.9	
	OBD[52]	4.1	0.2	−4.4
	DCMIX1[54]	4.53 ± 0.6	−0.98 ± 0.2	
3	Benchmark[12]	12.8 ± 0.4	−5.8 ± 0.3	−7
4	This study	31.40 ± 4.5	−22.6 ± 7	−8.8 ± 2.5
	TC + SST[55]	19 ± 2	1.0	
	OBD[52]	21.7	−1.4	−20.3
	DCMIX1[54]	21.5 ± 0.6	−4.94 ± 0.4	
5	This study	44.56 ± 27	−44.8 ± 44	1.34 ± 17
	TC + SST[55]	15 ± 4	6	
	OBD[52]	19.5	−1.7	−17.7

In DP7, the mathematical modeling of the diffusive processes is simplified and can only be used if the Soret separation actually attains steady state at the end of the Soret phase of the runs.

2. Analysis of errors on the Soret coefficients

In Fig. 11, we have plotted in a S'_{T1}-S'_{T2} space the Soret coefficients obtained through the 7 data processing sequences together with the coefficients found in the literature.

A first observation is that, as discussed in Ref. 29, the coefficients obtained with different data processing methods are aligned in the S'_{T1}-S'_{T2} space. The error of the Soret coefficients has a remarkable property: instead of forming a radially uniform scattering cloud around the solution point $\{S'_{T1}, S'_{T2}\}$, it forms a very elongated ellipsoid, practically degenerated into a line. This means that all data processing sequences of Table II lead to consistent optical analysis of the experimental data. The dispersion on the obtained Soret coefficients is due to the conversion of optical quantities to concentration quantities. This step, in Eq. (7), requires inverting the matrix of optical contrast factors. This matrix is quite ill-conditioned, and the inversion amplifies a low optical noise into a large uncertainty in the concentrations. The orientation of the line in the S'_{T1}-S'_{T2} space is defined by the properties of the contrast factor matrix. In Ref. 61, it has been shown that the directions of the major and the minor axis of the uncertainty ellipsoid are given by the right-singular vectors of the contrast factor matrix. Based on this observation, it appears that DCMIX1 experimental data do not allow retrieving the ternary Soret coefficients with the same accuracy as for typical binary mixtures. However, these data provide a linear correlation between the Soret coefficients. By writing this correlation as

$$S'_{T,2} = AS'_{T,1} + \mathrm{B}, \tag{11}$$

we obtain the values of parameters A and B provided in Table VII.

This linear correlation corresponds essentially to the result of a single-color experiment. The second detection color narrows the solution space down from a straight line to a line segment, whose length depends on the condition number of the contrast factor matrix.

The consistency of the obtained results shows that, in general, all data processing sequences of Fig. 4 and Table II can reliably be used for the interpretation of ternary thermodiffusion experiments and we cannot point out clear criteria for preferring one data processing methodology over the others. On the other hand, such criteria may appear from a particularity of the raw data itself. The choice of a particular data processing methodology must be made on a case by case basis, depending on the characteristics of the experimental data.

3. Comparison with literature data

The comparison of our results with literature data,[32,52,54,55] as summarized in Fig. 11, shows that the coefficients found in previous publications are also located on the lines defined by Eq. (11). The coefficients of Refs. 32 and 54 were obtained from previous analysis of DCMIX1 data and computed using similar contrast factor matrices. These coefficients therefore unsurprisingly display the same trend as our results. Although, in the previous analysis, the authors did not notice and describe the scattering of $S'_{T,1}$ and $S'_{T,2}$ because

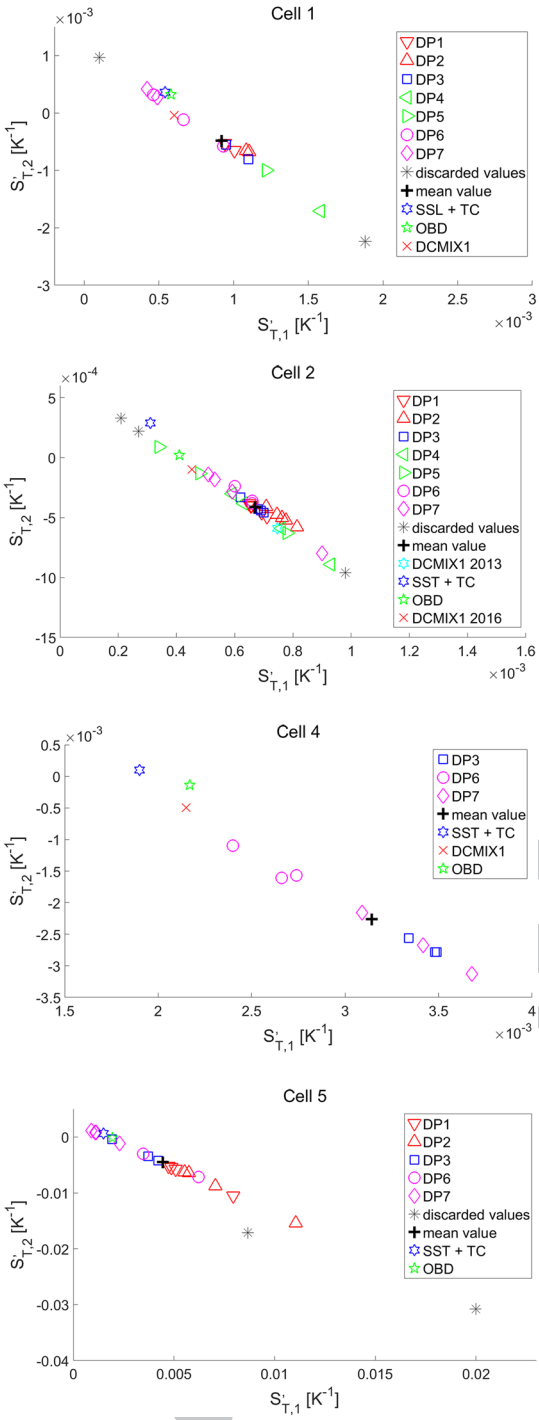

FIG. 11. Comparison of Soret coefficients with literature data, for DCMIX1 cells 1, 2, 4, and 5. The coefficients were obtained through data processing sequences DP1 to DP7 and compared with literature data, including coefficients obtained by the Optical Beam Deflection (OBD) technique,[52] by a previous analysis of DCMIX1 data,[32,54] and by combination of sliding symmetric tubes and thermogravitational column experiments (SST + TG).[55] All the obtained coefficients are aligned in the S'_{T1}-S'_{T2} space.

TABLE VII. Coefficients of the linear correlation between the Soret coefficients obtained in this study.

Cell	A	B
1	−1.6877	0.0011
2	−1.5856	0.0007
4	−1.5449	0.0026
5	−1.6347	26.2379

the conversion of refractive index into concentration in their algorithm was applied at an early stage, which resulted in overlooking the effect.

V. CONCLUSIONS

The Soret coefficients of a series of five ternary systems were performed under microgravity conditions aboard the International Space Station in the frame of the DCMIX1 experiment. In the present paper, we have detailed the experimental setup, the procedure, and the experimental data analysis. We have provided an extended review of the different possible data processing schemes used in the interpretation of digital interferometric ternary thermodiffusion experiments. We have shown that different choices of image processing algorithm and mathematical modeling of the experiments are possible and lead to consistent results. We have observed that the measured Soret coefficients are aligned in the $S'_{T,1}$-$S'_{T,2}$ space and that there remains an indetermination on the values of the measured Soret coefficients due to the ill-conditioned matrix of optical contrast factors. We have derived a linear correlation between the Soret coefficients for each ternary system. These correlations allow for an experimental validation of the Soret coefficients measured by OBD[52] and by the combination SST + TG[55] in ground conditions by comparison with the results of the microgravity DCMIX1 experiment.

From the comparison with literature data, we can conclude the consistency of the data obtained from the SODI instrument by different data processing approaches. Besides, we have compared our results with coefficients obtained in ground laboratories, by SST + TC in Ref. 55 or by OBD in Ref. 52. Those coefficients were computed using density and refractive index or refractive index at two different wavelengths (405 and 635 nm), respectively, for the concentration measurements. These techniques are therefore based on different contrast factor matrices, which provide some advantages for this particular system.

Nevertheless, all the coefficients, although measured with very different experimental techniques, using a variety of data processing approaches, and computed with different sets of contrast factors, are all located on the lines of Fig. 11. This observation suggests that the results of DCMIX1 allow for an experimental validation of the coefficients measured under gravity conditions in Refs. 52 and 55. As a general result, the Soret coefficients can be fixed in the direction of the short axis of the confidence ellipsoid with a high accuracy. How far they can be narrowed down in the perpendicular direction of the long axis very strongly depends on the contrast factor matrix and, hence, on the particular ternary mixture and the

employed experimental technique. For a mixture containing both aromatic and aliphatic compounds, it is advantageous to choose one wavelength in the blue, close to the UV-absorption of the delocalized π-electrons.[62] The DCMIX1 system belongs to this class of mixtures. But this advantage may be gone for systems without an aromatic compound. Also, the combination of density and refractive index detection, as employed in the thermogravitational column technique, can in certain cases profit from superior contrast factor matrices. Unfortunately, no perfect experimental technique exists that could cover all possible mixtures, and a change of the detection wavelengths is not feasible for the microgravity experiments.

ACKNOWLEDGMENTS

This work was supported by the SODiUM and DCMIX Prodex Programs funded by the Belgian federal Science Policy Office (SSTC). We are very grateful to European Space Agency for its constant support through this program and to F. Dubois and C. Minetti for support in image processing developments. W.K. and T.T. acknowledge support from the Deutsches Zentrum für Luft- und Raumfahrt (Grant Nos. 50WM1130 and 50WM1544). The study has been developed in the framework of the cooperative project DCMIX (Grant No. AO-2009-0858/1056) of the European Space Agency and the long-term program of scientific and applied research of the State Corporation "Rocosmos."

REFERENCES

[1] C. B. Mast and D. Braun, "Thermal trap for DNA replication," Phys. Rev. Lett. **104**, 188102 (2010).
[2] S. Duhr, S. Arduini, and D. Braun, Eur. Phys. J. E **15**, 277 (2004).
[3] G. Galliero, H. Bataller, F. Croccolo, R. Vermorel, P.-A. Artola, B. Rousseau, V. Vesovic, M. Bou-Ali, J. M. Ortiz de Zárate, S. Xu, K. Zhang, and F. Montel, Microgravity Sci. Technol. **28**(2), 79 (2016).
[4] P. M. Pancorbo, J. M. Ortiz de Zárate, H. Bataller, and F. Croccolo, Eur. Phys. J. E **40**, 22 (2017).
[5] F. Huang, P. Chakraborty, C. C. Lundstrom, C. Holmden, J. J. G. Glessner, S. W. Kieffer, and C. E. Lesher, Nature **464**, 396 (2010).
[6] K. Maeda, N. Shinyashiki, S. Yagihara, S. Wiegand, and R. Kita, J. Chem. Phys. **143**, 124504 (2015).
[7] J. K. Platten and P. Costesèque, Eur. Phys. J. E **15**, 235 (2004).
[8] J. K. Platten, J. Appl. Mech. **73**(1), 5 (2005).
[9] M. A. Rahman and M. Z. Saghir, Int. J. Heat Mass Transfer **73**, 693 (2014).
[10] S. Srinivasan and M. Z. Saghir, Int. J. Therm. Sci. **50**, 1125 (2011).
[11] W. Köhler and K. I. Morozov, J. Non-Equilib. Thermodyn. **41**, 151 (2016).
[12] M. M. Bou-Ali, A. Ahadi, D. Alonso de Mezquía, Q. Galand, M. Gebhardt, O. Khlybov, W. Köhler, M. Larrañaga, J.-C. Legros, T. Lyubimova, A. Mialdun, I. Ryzhkov, M. Z. Saghir, V. Shevtsova, and S. Van Vaerenbergh, Eur. Phys. J. E **38**, 30 (2015).
[13] S. R. de Groot and P. Mazur, *Non-Equilibrium Thermodynamics* (Dover, New York, 1984).
[14] S. Van Vaerenbergh, Microgravity Sci. Technol. **18**(3-4), 150 (2006).
[15] P. Kolodner, H. Willials, and C. Moe, J. Chem. Phys. **88**(10), 6512 (1988).
[16] V. Sechenyh, J. C. Legros, A. Mialdun, J. M. Ortiz de Zárate, and V. Shevtsova, J. Phys. Chem. B **120**, 535 (2016).
[17] S. Van Vaerenbergh, Z. Saghir, F. Montel, J. C. Legros, J. L. Daridon, J. Bickert, G. Galliero, and S. Churchill, High Pressure High Temp. **39**, 53 (2010).
[18] G. Galliero, H. Bataller, F. Croccolo, R. Vermorel, P.-A. Artola, B. Rousseau, V. Vesovic, M. Bou-Ali, J. M. Ortiz de Zárate, S. Xu, K. Zhang, and F. Montel, Microgravity Sci. Technol. **28**(2), 79 (2016).
[19] G. Galliero, H. Bataller, J.-P. Bazile, J. Diaz, F. Croccolo, H. Hoang, R. Vermorel, P.-A. Artola, B. Rousseau, V. Vesovic, M. Bou-Ali, J. M. Ortiz de Zárate, S. Xu, K. Zhang, F. Montel, A. Verga, and O. Minster, npj Microgravity **3**, 20 (2017).
[20] R. Taylor and R. Krishna, *Multicomponent Mass Transfer* (John Wiley & Sons, New York, 1993).
[21] W. M. Rutherford, J. Chem. Phys. **86**(9), 5217 (1987).
[22] S. Hartmann, G. Wittko, W. Köhler, K. I. Morozov, K. Albers, and G. Sadowski, Phys. Rev. Lett. **109**, 065901 (2012).
[23] S. Hartmann, G. Wittko, F. Schock, W. Groß, F. Lindner, W. Köhler, and K. I. Morozov, J. Chem. Phys. **141**, 134503 (2014).
[24] J. K. Platten, M. M. Bou Ali, J. F. Dutrieux, W. Köhler, C. Leppla, S. Wiegand, and G. Wittko, Philos. Mag. **83**, 1965 (2003).
[25] F. Croccolo, H. Bataller, and F. Scheffold, J. Chem. Phys. **137**, 234202 (2012).
[26] A. Mialdun, J.-C. Legros, V. Yasnou, V. Sechenyh, and V. Shevtsova, Eur. Phys. J. E **38**, 27 (2015).
[27] M. Gebhardt and W. Köhler, Eur. Phys. J. E **38**, 24 (2015).
[28] A. Ahadi, A. Khoshnevis, M. Dejmek, and Z. Saghir, "Influence of low and high frequency G-jitter vibrations on mixture during thermodiffusion experiment," in *Proceedings of the CASI ASTRO* (■, 2012), p. 12.
[29] R. Jurado, J. Pallarés, J. Gavaldà, and X. Ruiz, Int. J. Therm. Sci. **132**, 186 (2018).
[30] R. Jurado, J. Gavaldà, M. J. Simón, J. Pallarés, A. Laverón-Simavilla, X. Ruiz, and V. Shevtsova, Acta Astronaut. **129**, 345 (2016).
[31] R. Jurado, J. Pallarés, J. Gavaldà, and X. Ruiz, Int. J. Therm. Sci. **142**, 205 (2019).
[32] A. Ahadi, S. Van Vaerenbergh, and M. Z. Saghir, J. Chem. Phys. **138**(20), 204201 (2013).
[33] O. A. Khlybov, I. I. Ryzhkov, and T. P. Lyubimova, Eur. Phys. J. E **38**, 29 (2015).
[34] M. Lappa, C. Piccolo, G. Esposito, S. La Gala, D. Sorrentino, D. Giordano, G. De Chiara, G. Di Costanzo, R. Fortezza, and C. Albanese, in Proceedings of 63rd International Astronautical Congress, IAC-12.A2.5.9, 2012.
[35] A. Mialdun, I. Ryzhkov, O. Khlybov, T. Lyubimova, and V. Shevtsova, J. Chem. Phys. **148**, 044506 (2018).
[36] J. E. Greivenkamp and J. H. Bruning, "Phase shifting interferometers," in *Optical Shop Testing*, edited by D. Malacara (Wiley, New York, 1992), p. 501.
[37] J. Schmit, Proc. SPIE **1755**, 202 (1993).
[38] P. Hari Haran, B. F. Oreb, and T. Eiju, Appl. Opt. **26**(13), 2504 (1987).
[39] T. Kreis, *Handbook of Holographic Interferometry: Optical and Digital Methods* (Wiley, New York, 2005).
[40] T. Triller, H. Battaller, M. M. Bou-Ali, F. Croccolo, J. M. Ezquerro, Q. Galand, J. Gavalda, E. Lapeira, A. Laverón-Simavilla, T. Lyubimova, A. Mialdun, J. M. Ortiz de Zárate, J. Rodriguez, X. Ruiz, I. Ryzhkov, S. Van Vaerenbergh, and W. Köhler, Microgravity Sci. Technol. **30**(3), 295 (2018).
[41] Q. Kemao, Opt. Laser Eng. **45**(2), 304 (2007).
[42] L. Huang, Q. Kemao, B. pan, and A. Asundi, Opt. Laser Eng. **48**(2), 141 (2010).
[43] A. Mialdun and V. Shevtsova, J. Chem. Phys. **134**(4), 044524 (2011).
[44] W. Zhaoyang and H. Bongtae, Opt. Lett. **29**(14), 1671 (2004).
[45] D. C. Ghiglia and M. D. Pritt, *Two-Dimensional Phase Unwrapping, Theory, Algorithms and Software* (Wiley, New York, 1998).
[46] K. Itoh, "Analysis of the phase unwrapping algorithm," Appl. Opt. **21**(14), 2470 (1982).
[47] M. Costantini, IEEE Trans. Geosci. Electron. Remote Sens. **36**(3), 813 (1998).
[48] Q. Galand and S. Van Vaerenbergh, Eur. Phys. J. E **38**, 26 (2015).
[49] V. V. Sechenyh, J.-C. Legros, and V. Shevtsova, J. Chem. Thermodyn. **62**, 64 (2013).
[50] V. Shevtsova, V. V. Sechenyh, A. Nepomnyashchy, and J.-C. Legros, Philos. Mag. **91**(26), 3498 (2011).
[51] A. Mialdun, V. Yasnou, V. Shevtsova, A. Königer, W. Köhler, D. Alonso de Mezquía, and M. M. Bou Ali, J. Chem. Phys. **136**, 244512 (2012).
[52] M. Gebhardt and W. Köhler, J. Chem. Phys. **143**, 164511 (2015).
[53] M. Gebhardt, W. Köhler, A. Mialdun, V. Yasnou, and V. Shevtsova, J. Chem. Phys. **138**(11), 114503 (2013).
[54] A. Ahadi and M. Z. Saghir, Exp. Therm. Fluid Sci. **74**, 296 (2016).
[55] M. Larrañaga, M. M. Bou-Ali, I. Lizarraga, J. A. Madariaga, and C. Santamaria, J. Chem. Phys. **143**, 024202 (2015).

[56]M. Larrañaga, M. M. Bou-Ali, D. Alonso de Mezquía, D. A. S. Rees, J. A. Madariaga, C. Santamaría, and J. K. Platten, Eur. Phys. J. E **38**, 28 (2015).
[57]V. Shevtsova, Y. Gaponenko, V. Sechenyh, D. Melnikov, T. Lyubimova, and A. Mialdun, J. Fluid Mech. **767**, 290 (2015).
[58]A. Mialdun and V. Shevtsova, J. Chem. Phys. **143**, 224902 (2015).
[59]S. Van Vaerenbergh and J.-C. legros, "Kinetics of the Soret effect: Transient in the transport process," Phys. Rev. A **41**, 6727 (1990).
[60]Q. Galand, "Experimental investigation of the diffusive properties of ternary liquid systems," Ph.D. thesis, Université libre de Bruxelles, Brussels, 2012.
[61]T. Triller, D. Sommermann, M. Schraml, F. Sommer, E. Lapeira, M. M. Bou-Ali, and W. Köhler, Eur. Phys. J. E **42**, 27 (2019).
[62]A. Königer, H. Wunderlich, and W. Köhler, J. Chem. Phys. **132**, 174506 (2010).